
REGRESSION ANALYSIS OF ELLIPTICALLY SYMMETRIC DIRECTIONAL DATA

A PREPRINT

Zehao Yu
 Department of Statistics
 University of South Carolina
 Columbia, SC 29201
 zehaoy@email.sc.edu

Xianzheng Huang
 Department of Statistics
 University of South Carolina
 Columbia, SC 29201
 huang@stat.sc.edu

ABSTRACT

A comprehensive toolkit is developed for regression analysis of directional data based on a flexible class of angular Gaussian distributions. Informative testing procedures for isotropy and covariate effects on the directional response are proposed. Moreover, a prediction region that achieves the smallest volume in a class of ellipsoidal prediction regions of the same coverage probability is constructed. The efficacy of these inference procedures is demonstrated in simulation experiments. Finally, this new toolkit is used to analyze directional data originating from a hydrology study and a bioinformatics application.

Keywords Angular Gaussian · Hypersphere · Isotropy · Prediction region

1 Introduction

Directional data naturally arise in many scientific disciplines, such as flight directions of migrating birds, the directions of wind and waves in the ocean, and geomagnetic field directions. These examples of directional data as the original form of observed data are typically of low dimensions. High dimensional directional data typically result from preprocessing high dimensional features collected in genetic study (Banerjee et al., 2005), computer vision (Ryali et al., 2013), and text analysis (Ennajari et al., 2021), among many other research fields. In these instances, the raw data vectors in some d -dimensional Euclidean space \mathbb{R}^d are often normalized to lie on a hypersphere $\mathbb{S}^{d-1} = \{\mathbf{y} \in \mathbb{R}^d : \|\mathbf{y}\| = 1\}$, where $\|\mathbf{y}\|$ denotes the Euclidean norm of \mathbf{y} .

Regression analysis of directional data is relatively underdeveloped compared to regression analysis of response data in the linear (Euclidean) space. One of the most notable early developments of regression models for directional data is given by Johnson and Wehrly (1978), who formulated parametric models for the joint distribution of a circular response (i.e., $d = 2$) and a linear covariate. Later, Presnell et al. (1998) introduced the spherically projected multivariate linear model based on the projected Gaussian distribution for the circular response with a mean direction depending on covariates linearly. Mimicking the least squares method in regression analysis for a linear response, Lund (1999) proposed a least circular-distance method for regression analysis of a circular response. Scealy and Wood (2019) proposed a transformation of the von Mises-Fisher distribution to study paleomagnetic data, following which they built regression models using the proposed directional distribution. Paine et al. (2018) proposed the elliptically symmetric angular Gaussian distribution (ESAG), focusing on directional data on \mathbb{S}^2 . In a follow-up work (Paine et al., 2020), the authors formulated regression models based on ESAG of low dimensions.

The formulation of ESAG results from imposing constraints on the mean $\boldsymbol{\mu}$ and variance-covariance matrix \mathbf{V} of a multivariate Gaussian distribution $\mathcal{N}_d(\boldsymbol{\mu}, \mathbf{V})$ to resolve the identifiability issue. Such an identifiability issue emerges inevitably when normalizing a multivariate Gaussian vector to yield an angular Gaussian random variable, since two Gaussian vectors, \mathbf{W} and $c\mathbf{W}$, are normalized to the same vector when $c > 0$, yet they follow different Gaussian distributions whenever $c \neq 1$. For most angular Gaussian distributions, constraints are imposed on \mathbf{V} that often translate to stringent assumptions on the resultant directional distribution. The constraints on $\boldsymbol{\mu}$ and \mathbf{V} that lead to ESAG give rise to a probability density function (pdf) that does not involve a complicated normalization constant, and the resultant

distribution remains flexible in that it is not limited to isotropic distributions. These are virtues of ESAG that make it stand out among many existing named directional distributions. Section 2 provides a brief review of ESAG and its parameterization that facilitates regression analysis of directional data. We then address three inference problems that are theoretically and practically important in the context of directional distributions and regression analysis. More specifically, Section 3 presents a novel diagnostic test to check isotropy. An isotropic distribution supported on a hypersphere is rotation-invariant, that is, rotating an isotropic random vector does not change its distribution. Isotropy is similar to symmetry for a distribution supported on a linear space, and thus testing isotropy is loosely parallel to testing the symmetry of a distribution. In Section 4, we propose methods for testing covariate-dependence of ESAG model parameters. Section 5 reports simulation studies for assessing the operating characteristics of the proposed testing procedures. Section 6 provides prediction regions of the directional response. We apply these new inference procedures to two real-life applications in Section 7. Section 8 recapitulates the contributions of our study and points out some limitations of the proposed regression framework that motivate follow-up research.

2 The ESAG regression model and likelihood-based inference

2.1 The model and data

A random variable \mathbf{Y} supported on \mathbb{S}^{d-1} follows an angular Gaussian distribution, $\text{AG}(\boldsymbol{\mu}, \mathbf{V})$, if $\mathbf{Y} = \mathbf{W}/\|\mathbf{W}\|$ with $\mathbf{W} \sim \mathcal{N}_d(\boldsymbol{\mu}, \mathbf{V})$. The parameter $\boldsymbol{\mu}$ in $\text{AG}(\boldsymbol{\mu}, \mathbf{V})$ is the mean direction of \mathbf{Y} . To guarantee the identifiability of the distribution $\text{AG}(\boldsymbol{\mu}, \mathbf{V})$, assumptions on $(\boldsymbol{\mu}, \mathbf{V})$ are needed to avoid overparameterization. For example, Presnell et al. (1998) assumed $\mathbf{V} = \mathbf{I}_d$ that leads to an isotropic directional distribution, where \mathbf{I}_d is the d -dimensional identity matrix. Less stringent assumptions are also considered, for example, in Wang and Gelfand (2013) where a sub-block of \mathbf{V} is assumed known. We adopt the ESAG distribution (Paine et al., 2018) resulting from imposing the following constraints that we refer to as ESAG constraints henceforth, $\mathbf{V}\boldsymbol{\mu} = \boldsymbol{\mu}$ and $\det(\mathbf{V}) = 1$, where $\det(\mathbf{V})$ denotes the determinant of \mathbf{V} . These constraints leave more room for flexible modeling of \mathbf{Y} than most previously considered constraints, at the price of creating a more complex constrained parameter space. We recently reparameterized ESAG by introducing constraint-free parameters $\boldsymbol{\gamma} \in \mathbb{R}^{(d-2)(d+1)/2}$ so that \mathbf{V} that satisfies ESAG constraints can be determined by $(\boldsymbol{\mu}, \boldsymbol{\gamma})$ via an eigendecomposition (Yu and Huang, 2024). Henceforth, we use $\mathbf{Y} \sim \text{ESAG}(\boldsymbol{\mu}, \boldsymbol{\gamma})$ to refer to $\mathbf{Y} \sim \text{AG}(\boldsymbol{\mu}, \mathbf{V})$ with ESAG constraints imposed on $(\boldsymbol{\mu}, \mathbf{V})$.

The benefits of modeling ESAG via constraint-free parameters are at least twofold. First, maximum likelihood estimation of model parameters becomes more straightforward than directly estimating $(\boldsymbol{\mu}, \mathbf{V})$ subject to the nonlinear ESAG constraints. Second, a covariate-dependent ESAG can be easily formulated without introducing link functions to relate covariates to constrained model parameters as done in earlier regression models for directional responses (Lund, 1999; Scealy and Welsh, 2011, 2017). In this study, we consider an ESAG regression model specified by $\mathbf{Y}|\mathbf{X} \sim \text{ESAG}(\boldsymbol{\mu} = \boldsymbol{\alpha}_0 + \mathbf{A}_1\mathbf{X}, \boldsymbol{\gamma} = \boldsymbol{\beta}_0 + \mathbf{B}_1\mathbf{X})$, where $\mathbf{X} = (X_1, \dots, X_q)^\top$ is the q -dimensional covariate vector, $\boldsymbol{\alpha}_0$ is the intercept for modeling $\boldsymbol{\mu}$, $\mathbf{A}_1 = [\boldsymbol{\alpha}_1 | \dots | \boldsymbol{\alpha}_q]$ is the $d \times q$ matrix of regression coefficients representing covariates effects on $\boldsymbol{\mu}$, $\boldsymbol{\beta}_0$ is the intercept parameter in $\boldsymbol{\gamma}$, and $\mathbf{B}_1 = [\boldsymbol{\beta}_1 | \dots | \boldsymbol{\beta}_q]$ is the $(d-2)(d+1)/2 \times q$ matrix of covariates effects on $\boldsymbol{\gamma}$, in which $\boldsymbol{\alpha}_k \in \mathbb{R}^d$ and $\boldsymbol{\beta}_k \in \mathbb{R}^{(d-2)(d+1)/2}$, for $k = 0, 1, \dots, q$.

Suppose the observed data include directional responses $\{\mathbf{Y}_1, \dots, \mathbf{Y}_n\}$ from n independent experimental units along with their covariates data $\{\mathbf{X}_1, \dots, \mathbf{X}_n\}$. Similar to the treatment on covariates data in Scealy and Wood (2019), we standardize covariates data via $(X_{i,k} - X_{(1),k})/(X_{(n),k} - X_{(1),k}) + 1$, for $i = 1, \dots, n$, where $X_{(1),k}$ and $X_{(n),k}$ are the minimum and maximum order statistics corresponding to covariate X_k , for $k = 1, \dots, q$. The resultant standardized covariates data are more comparable in scale with the response of a unit Euclidean norm, which helps to stabilize the numerical implementation of maximum likelihood estimation without distorting the underlying association between the response and covariates. With a slight abuse of notation, we use $\{\mathbf{X}_i\}_{i=1}^n$ to refer to the standardized covariates data.

2.2 Maximum likelihood estimation

To parameterize \mathbf{V} in $\text{AG}(\boldsymbol{\mu}, \mathbf{V})$ to satisfy ESAG constraints, we introduced longitude and latitude angle parameters to specify eigenvectors of \mathbf{V} after $\boldsymbol{\mu}$ is specified. We showed that $\boldsymbol{\gamma}$ or a certain subvector of it being zero amounts to some latitude angles falling on the boundary of 0 or π and some other latitude and longitude angles being non-identifiable (see Appendix B in Yu and Huang, 2024, for details). This suggests violations of regularity conditions in the context of drawing likelihood-based inference for model parameters even though the parameter space of $\text{ESAG}(\boldsymbol{\mu}, \boldsymbol{\gamma})$ is the entire real space $\mathbb{R}^{(d-1)(d+2)/2}$. The irregularity carries over to the ESAG regression model. As a result, maximum likelihood estimators (MLE) of some regression coefficients may converge in distribution to Gaussian at a slower rate than \sqrt{n} , or may not be asymptotically Gaussian, depending on where the true model parameters fall in the parameter space. Regardless, numerical implementation maximum likelihood estimation is straightforward under the current

parameterization of ESAG, as demonstrated in our earlier work (and thus omitted here), and a simple resample-based bootstrap procedure can be used to quantify the uncertainty of the MLEs.

When it comes to hypothesis testing, the conventional likelihood ratio test (LRT) is inadequate when regularity conditions are not satisfied because the asymptotic null distribution of a likelihood ratio (LR) statistic is no longer a χ^2 (Chernoff, 1954). Most existing solutions to this complication with the LRT aim at estimating the exact distribution of LR or its limiting distribution under the null using some simulation-based methods, such as the method proposed by Drton (2009) and the approach developed in Mitchell et al. (2019). Instead of using LR, we propose different test statistics that exploit unique properties of the ESAG distribution. These are elaborated in the next two sections, one focusing on tests for isotropy, and the other considering tests for covariate dependence of $\boldsymbol{\mu}$ and $\boldsymbol{\gamma}$.

3 Hypothesis testing for isotropy

If \mathbf{Y} follows an isotropic distribution, then $\mathbf{R}\mathbf{Y}$ and \mathbf{Y} are identically distributed for any given $d \times d$ rotation matrix \mathbf{R} . By the parameterization of \mathbf{V} via $\boldsymbol{\gamma}$, ESAG($\boldsymbol{\mu}, \boldsymbol{\gamma}$) is isotropic when $\boldsymbol{\gamma} = \mathbf{0}$, which gives $\mathbf{V} = \mathbf{I}_d$. Hence, testing isotropy is relevant to inferring correlations of the components in \mathbf{W} , i.e., the pre-normalization version of \mathbf{Y} , and also relates to model selection between the more parsimonious isotropic ESAG and a generic ESAG distribution. In what follows, we propose a strategy for testing the null hypothesis $H_0^{(\mathbf{V})} : \mathbf{Y} \sim \text{ESAG}(\boldsymbol{\mu}, \boldsymbol{\gamma} = \mathbf{0})$, where potential dependence of $\boldsymbol{\mu}$ on covariates \mathbf{X} is suppressed for notational simplicity. The proposed strategy is motivated by the properties of the MLE for the concentration parameter in the presence of model misspecification.

3.1 Concentration estimation

For ESAG($\boldsymbol{\mu}, \boldsymbol{\gamma}$), $\|\boldsymbol{\mu}\|$ quantifies the overall concentration of the distribution, with \mathbf{V} controlling the variation in different subspaces on the unit sphere. Visually, the shape of a data cloud from an isotropic ESAG resembles a $(d - 1)$ -dimensional sphere, whereas the shape of a data cloud from an anisotropic ESAG is like a $(d - 1)$ -dimensional ellipsoid. Intuitively, when fitting an isotropic ESAG model to data from an anisotropic distribution, one essentially tries to find a ball that can most compactly contain an ellipsoid. To accomplish this, the radius of the ball tends to approach that of the longest axis of the ellipsoid, leading to a lower concentration of the fitted isotropic ESAG compared to the concentration of the true anisotropic distribution. In the context of model comparison, two ESAG distributions, ESAG($\boldsymbol{\mu}_1, \boldsymbol{\gamma}_1 = \mathbf{0}$) and ESAG($\boldsymbol{\mu}_2, \boldsymbol{\gamma}_2 \neq \mathbf{0}$), are more alike when $\|\boldsymbol{\mu}_1\| < \|\boldsymbol{\mu}_2\|$ than when $\|\boldsymbol{\mu}_1\| \geq \|\boldsymbol{\mu}_2\|$. We demonstrate this phenomenon next by exploiting the properties of MLEs in the presence of model misspecification.

Let P denote a generic ESAG distribution with pdf $P(\mathbf{Y}; \boldsymbol{\mu}_a, \boldsymbol{\gamma}_a)$, which specifies the true data-generating mechanism. Let Q denote an isotropic ESAG distribution with pdf $Q(\mathbf{Y}; \boldsymbol{\mu})$. The Kullback–Leibler divergence of Q from P is defined as $D_{\text{KL}}(P\|Q; \boldsymbol{\mu}) = E_P[\log\{P(\mathbf{Y}; \boldsymbol{\mu}_a, \boldsymbol{\gamma}_a)/Q(\mathbf{Y}; \boldsymbol{\mu})\}]$, where the subscript “ P ” signifies that the expectation is with respect to the distribution P . Under regularity conditions (White, 1982), if one fits the model Q to data from P , then the MLE for $\boldsymbol{\mu}$ converges in probability to $\boldsymbol{\mu}_0 = \text{argmin}_{\boldsymbol{\mu}} D_{\text{KL}}(P\|Q; \boldsymbol{\mu}) = \text{argmax}_{\boldsymbol{\mu}} E_P\{\log Q(\mathbf{Y}; \boldsymbol{\mu})\}$. We show next that $\|\boldsymbol{\mu}_0\| \leq \|\boldsymbol{\mu}_a\|$, or, equivalently, in the presence of model misspecification (i.e., $P \neq Q$), $E_P\{\log Q(\mathbf{Y}; \boldsymbol{\mu})\}$ is maximized when the ratio of concentrations (RoC) $\|\boldsymbol{\mu}_a\|/\|\boldsymbol{\mu}_0\|$ exceeds one. To highlight the concentration, we view $\boldsymbol{\mu}_a = c_a \mathbf{R}_a \boldsymbol{\mu}^*$ and $\boldsymbol{\mu}_0 = c_0 \mathbf{R}_0 \boldsymbol{\mu}^*$ for some rotation matrices, \mathbf{R}_a and \mathbf{R}_0 , and some positive constants, c_a and c_0 , where $\boldsymbol{\mu}^*$ is a unit vector. In other words, $\boldsymbol{\mu}_a$ and $\boldsymbol{\mu}_0$ may differ in concentration, quantified by c_a and c_0 respectively, or differ in orientation when $\mathbf{R}_a \neq \mathbf{R}_0$. Using this factorization of the mean direction parameter, we have $\|\boldsymbol{\mu}_a\|/\|\boldsymbol{\mu}_0\| = c_a/c_0$ since $\|\mathbf{R}_a \boldsymbol{\mu}^*\|/\|\mathbf{R}_0 \boldsymbol{\mu}^*\| = 1$. Now we re-express the density $P(\cdot; \boldsymbol{\mu}_a, \boldsymbol{\gamma}_a)$ as $P(\cdot; c_a, \mathbf{R}_a, \boldsymbol{\gamma}_a)$, and similarly write the density $Q(\cdot; \boldsymbol{\mu})$ as $Q(\cdot; c, \mathbf{R})$, where the dependence of these distributions on $\boldsymbol{\mu}^*$ is suppressed because the value of $\boldsymbol{\mu}^*$ remains the same for all ESAG distributions under this formulation of the mean direction parameter. Without loss of generality, let $\boldsymbol{\mu}^* = \boldsymbol{\mu}_a/\|\boldsymbol{\mu}_a\|$. With this choice of $\boldsymbol{\mu}^*$, we have $c_a = \|\boldsymbol{\mu}_a\|$ and $\mathbf{R}_a = \mathbf{I}_d$. Fitting Q to data from P now amounts to, in limit as $n \rightarrow \infty$, maximizing $E_P\{\log Q(\mathbf{Y}; c, \mathbf{R})\}$ with respect to (c, \mathbf{R}) , which cannot be done analytically but can be simulated using large samples.

To simulate this maximization problem, we generate a random sample of size $n = 10^4$ from $P(\cdot; c_a, \mathbf{R}_a, \boldsymbol{\gamma}_a)$ for a $\boldsymbol{\mu}_a$ we specify, and $\boldsymbol{\gamma}_a$ taking one of the following three values, $\boldsymbol{\gamma}^{(1)} = \mathbf{0}$, non-zero $\boldsymbol{\gamma}^{(2)}$ and $\boldsymbol{\gamma}^{(3)}$, with the first value creating a scenario where $P = Q$, and the latter two creating increasing degree of anisotropy in P . We then use the log-likelihood function $\ell(c, \mathbf{R}) = n^{-1} \sum_{i=1}^n \log Q(\mathbf{Y}_i; c, \mathbf{R})$ as an empirical version of $E_P\{\log Q(\mathbf{Y}; c, \mathbf{R})\}$ to demonstrate that $c_a/c^* > 1$ when $\boldsymbol{\gamma}_a \neq \mathbf{0}$, where $c^* = \text{argmax}_{c>0} \ell(c, \mathbf{R}^*)$ for some arbitrary rotation matrix \mathbf{R}^* . For concreteness, we consider three values for \mathbf{R}^* given by $\mathbf{R}^{(1)} = \mathbf{R}_a$, $\mathbf{R}^{(2)} \neq \mathbf{R}_a$, and $\mathbf{R}^{(3)}$ that deviates from \mathbf{R}_a further than $\mathbf{R}^{(2)}$ does.

The top panel of Figure 1 depicts $\ell(c, \mathbf{R}^{(1)})$ as a function of $\text{RoC} = c_a/c$ when the data-generating mechanism P has γ_a set at $\gamma^{(1)} = \mathbf{0}$ (isotropy), $\gamma^{(2)} \neq \mathbf{0}$ (mild anisotropy), and $\gamma^{(3)}$ that deviates from zero even further (severe anisotropy), respectively. With $\mathbf{R}^{(1)} = \mathbf{R}_a$, the mean directions of P and Q have the same orientation. When P is isotropic, $E_P\{\log Q(\mathbf{Y}; c, \mathbf{R}^{(1)})\}$ is expected to be maximized at $c^* = c_a$, resulting in $D_{\text{KL}}(P\|Q; \boldsymbol{\mu}_0) = 0$. This is indeed (empirically) justified by the curve of $\ell(c; \mathbf{R}^{(1)})$ that reaches its peak at around $\text{RoC} = c_a/c^* = 1$. Once P exhibits anisotropy by having γ_a deviating from $\mathbf{0}$, one witnesses a drop in the likelihood $\ell(c, \mathbf{R}^{(1)})$, which is maximized at some RoC that exceeds 1, indicating that $c^* < c_a$. The inflation in RoC , i.e., the attenuation in c^* , becomes more substantial as γ_a deviates from $\mathbf{0}$ further. This implies that misspecifying γ in the ESAG distribution by assuming isotropy can be manifested in a larger-than-1 RoC . The bottom two panels in Figure 1 show $\ell(c, \mathbf{R}^{(2)})$ and $\ell(c, \mathbf{R}^{(3)})$ versus RoC , where all the previously observed phenomena for $\ell(c, \mathbf{R}^{(1)})$ remain except for that, even with γ_a set at $\mathbf{0}$, $\ell(c, \mathbf{R}^*)$ is also maximized when RoC is larger than 1.

Comparing the three panels in Figure 1 reveals a clear trend of RoC increasing as model misspecification becomes more severe by having γ_a further away from zero or having the orientation of $\boldsymbol{\mu}_a$ mismatch more with the orientation of $\boldsymbol{\mu}_0$. The latter observation suggests that RoC can be used to test assumptions regarding $\boldsymbol{\mu}$ as well, which is a point we come back to in a later section on testing assumptions on the mean direction parameter.

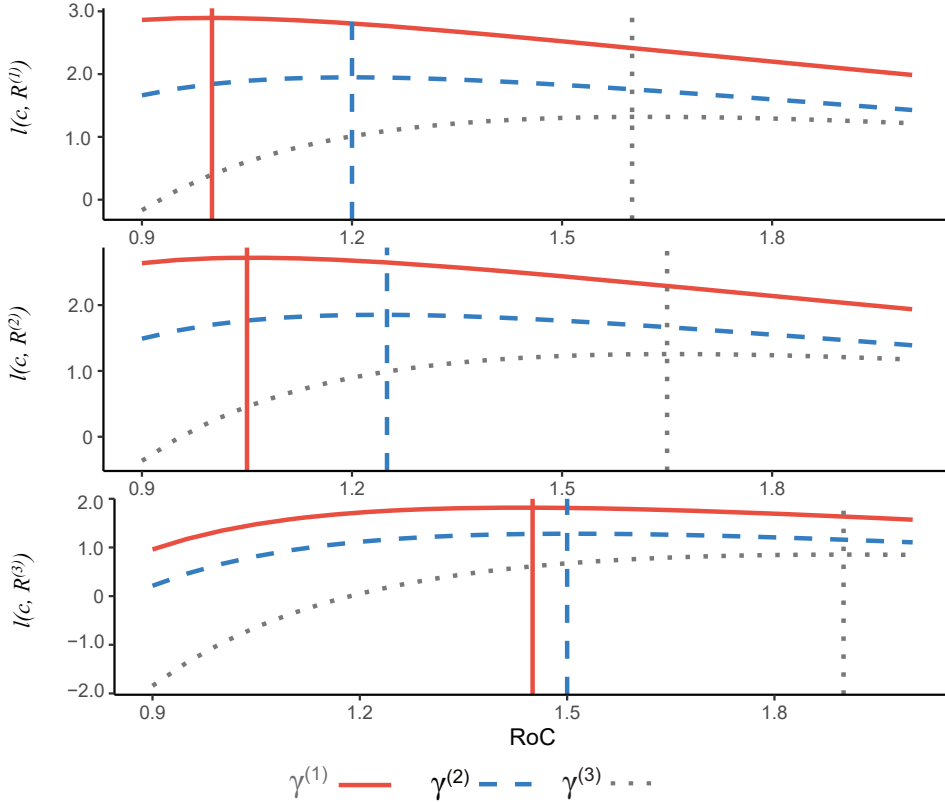


Figure 1: The empirical version of $E_P\{\log Q(\mathbf{Y}; c, \mathbf{R})\}$, $\ell(c, \mathbf{R})$, based on a random sample of size $n = 10^4$ from an isotropic ESAG (red lines), a mildly anisotropic ESAG with $\gamma = \gamma^{(2)} \neq \mathbf{0}$ (blue dashed lines), and an anisotropic ESAG with $\gamma = \gamma^{(3)}$ deviating from $\mathbf{0}$ even further (gray dotted lines), versus RoC when \mathbf{R} is set at $\mathbf{R}^{(1)} = \mathbf{I}_d$ (top panel), $\mathbf{R}^{(2)} \neq \mathbf{I}_d$ (middle panel), and $\mathbf{R}^{(3)}$ that deviates from \mathbf{I}_d even more (bottom). Vertical lines mark the value of RoC where the corresponding function $\ell(c, \mathbf{R})$ is maximized.

3.2 Testing isotropy based on concentration estimation

Inspired by the above findings regarding concentration estimation, we propose the statistic for testing isotropy defined by

$$\text{RoC} = \frac{1}{n} \sum_{i=1}^n \frac{\|\hat{\boldsymbol{\mu}}_{ai}\|}{\|\hat{\boldsymbol{\mu}}_{0i}\|}, \quad (3.1)$$

where $\hat{\boldsymbol{\mu}}_{0i}$ is the restricted MLE of the mean direction of \mathbf{Y}_i given \mathbf{X}_i under $H_0^{(\mathbf{V})}$, and $\hat{\boldsymbol{\mu}}_{ai}$ is the unrestricted MLE under the alternative hypothesis that allows anisotropy. If the true data-generating mechanism is consistent with $H_0^{(\mathbf{V})}$, then RoC is expected to be close to one; otherwise, RoC tends to be larger than one.

Algorithm 1 below gives the parametric bootstrap procedure to estimate the p -value associated with RoC to assess its statistical significance. The goal of the bootstrap procedure is to estimate the null distribution of RoC by simulating realizations of RoC under the null. To this end, we repeatedly compute RoC based on data generated from an isotropic ESAG distribution $\hat{Q}(\cdot; \hat{\boldsymbol{\mu}}_{0i})$ for the i -th experimental unit, for $i = 1, \dots, n$. This distribution is an estimate of Q that is closest to the unknown true model P for each experimental unit. An estimated p -value can then be obtained by comparing the RoC computed based on the raw data with the simulated RoC's. As seen here and in the testing procedures proposed later for other purposes, the distribution of a test statistic under any hypothesized ESAG model can be easily approximated via parametric bootstrap because it is straightforward to simulate data from any ESAG distribution, which is yet another virtue of the ESAG distribution family and the constrain-free parameterization.

Algorithm 1 Hypothesis testing for isotropy based on RoC defined in (3.1)

- 1: **procedure** COMPUTE RoC BASED ON THE OBSERVED DATA
 - 2: Input data $\{(\mathbf{Y}_i, \mathbf{X}_i)\}_{i=1}^n$, find the restricted MLE $\hat{\boldsymbol{\mu}}_{0i}$ under $H_0^{(\mathbf{V})}$ and the unrestricted MLE $\hat{\boldsymbol{\mu}}_{ai}, \hat{\gamma}_{ai}$, for $i = 1, \dots, n$.
 - 3: Compute the test statistic $\text{RoC} = (1/n) \sum_{i=1}^n \|\hat{\boldsymbol{\mu}}_{ai}\| / \|\hat{\boldsymbol{\mu}}_{0i}\|$.
 - 4: **end procedure**
 - 5: **procedure** BOOTSTRAP PROCEDURE TO ESTIMATE THE NULL DISTRIBUTION OF RoC
 - 6: Set $B =$ number of bootstraps
 - 7: Initiate $s = 0$
 - 8: **for** b in $1, \dots, B$ **do**
 - 9: Generate the b -th bootstrap sample $\{\mathbf{Y}_i^{(b)}\}_{i=1}^n$, where $\mathbf{Y}_i^{(b)} | \mathbf{X}_i \sim \text{ESAG}(\hat{\boldsymbol{\mu}}_{0i}, \boldsymbol{\gamma}_i = \mathbf{0})$, for $i = 1, \dots, n$.
 - 10: Repeat Steps 2–3 using data $\{(\mathbf{Y}_i^{(b)}, \mathbf{X}_i)\}_{i=1}^n$. Denote the resultant value of RoC as $\text{RoC}^{(b)}$.
 - 11: **if** $\text{RoC}^{(b)} > \text{RoC}$ **then** $s = s + 1$
 - 12: **end for**
 - 13: Output s/B as an estimated p -value associated with RoC from Step 3.
 - 14: **end procedure**
-

4 Tests for covariates effects

4.1 Testing covariates dependence of $\boldsymbol{\mu}$

For a directional response, a practically interesting question is whether or not its mean direction depends on covariates. For concreteness, let us consider testing the null $H_0^{(\boldsymbol{\mu})} : \mathbf{Y} | \mathbf{X} \sim \text{ESAG}(\boldsymbol{\mu} = \boldsymbol{\alpha}_0, \boldsymbol{\gamma} = \boldsymbol{\beta}_0 + \mathbf{B}_1 \mathbf{X})$ versus the alternative $H_1 : \mathbf{Y} | \mathbf{X} \sim \text{ESAG}(\boldsymbol{\mu} = \boldsymbol{\alpha}_0 + \mathbf{A}_1 \mathbf{X}, \boldsymbol{\gamma} = \boldsymbol{\beta}_0 + \mathbf{B}_1 \mathbf{X})$. If the alternative is true with $\mathbf{A}_1 \neq \mathbf{0}$, the fitted $\boldsymbol{\mu}$ under the null, denoted by $\hat{\boldsymbol{\mu}}_0$, is expected to differ from the fitted value that allows covariates dependence of $\boldsymbol{\mu}$, denoted by $\hat{\boldsymbol{\mu}}_a$. The difference can lie in their norms, i.e., concentrations, or in their directions. This motivates the following test statistic that captures both sources of discrepancies,

$$D = \frac{1}{n} \sum_{i=1}^n \left(2 - \frac{\hat{\boldsymbol{\mu}}_{0i}^\top \hat{\boldsymbol{\mu}}_{ai}}{\|\hat{\boldsymbol{\mu}}_{0i}\| \|\hat{\boldsymbol{\mu}}_{ai}\|} \right) \frac{\|\hat{\boldsymbol{\mu}}_{ai}\|}{\|\hat{\boldsymbol{\mu}}_{0i}\|}, \quad (4.1)$$

where, for the i -th data point, $\hat{\boldsymbol{\mu}}_{0i}$ is the restricted MLE obtained under the null that assumes covariate-independent $\boldsymbol{\mu}$, and $\hat{\boldsymbol{\mu}}_{ai}$ is the unrestricted MLE obtained under the alternative. In (4.1), $\hat{\boldsymbol{\mu}}_{0i}^\top \hat{\boldsymbol{\mu}}_{ai} / (\|\hat{\boldsymbol{\mu}}_{0i}\| \|\hat{\boldsymbol{\mu}}_{ai}\|)$ is known as the cosine similarity between two vectors, $\hat{\boldsymbol{\mu}}_{0i}$ and $\hat{\boldsymbol{\mu}}_{ai}$, which is equal to 1 if they have the same direction, and is equal to -1 if the directions are opposite. Hence the first factor in the summand in (4.1) quantifies the dissimilarity in direction between $\hat{\boldsymbol{\mu}}_{0i}$ and $\hat{\boldsymbol{\mu}}_{ai}$. The second factor of the summand in (4.1) contrasts the concentrations of the two estimates for

μ as in RoC. By construction, under the null $H_0^{(\mu)}$, D is expected to be close to 1; and a realization of D that is much larger than 1 can imply the observed data coming from a model that violates of the null.

Algorithm 2 provides detailed steps for implementing the test based on the newly proposed test statistic, where we again use a parametric bootstrap procedure to estimate the p -value associated with D .

Algorithm 2 Hypothesis testing regarding μ based on D defined in (4.1)

```

1: procedure COMPUTE  $D$  BASED ON THE OBSERVED DATA
2:   Input data  $\{(\mathbf{Y}_i, \mathbf{X}_i)\}_{i=1}^n$ , find the restricted MLEs  $\hat{\mu}_{0i}$  and  $\hat{\gamma}_{0i}$ , and the unrestricted MLEs  $\hat{\mu}_{1i}$  and  $\hat{\gamma}_{1i}$ , for  $i = 1, \dots, n$ .
3:   Compute  $D = (1/n) \sum_{i=1}^n \{2 - (\hat{\mu}_{0i}^\top \hat{\mu}_{1i}) / (\|\hat{\mu}_{0i}\| \|\hat{\mu}_{1i}\|)\} (\|\hat{\mu}_{1i}\| / \|\hat{\mu}_{0i}\|)$ .
4: end procedure
5: procedure BOOTSTRAP PROCEDURE TO ESTIMATE THE NULL DISTRIBUTION OF  $D$ 
6:   Set  $B =$  number of bootstraps
7:   Initiate  $s = 0$ 
8:   for  $b$  in  $1, \dots, B$  do
9:     Generate the  $b$ -th bootstrap sample  $\{\mathbf{Y}_i^{(b)}\}_{i=1}^n$ , where  $\mathbf{Y}_i^{(b)} | \mathbf{X}_i \sim \text{ESAG}(\hat{\mu}_{0i}, \hat{\gamma}_{0i})$ , for  $i = 1, \dots, n$ .
10:    Repeat Steps 2–3 using data  $\{(\mathbf{Y}_i^{(b)}, \mathbf{X}_i)\}_{i=1}^n$ . Denote the resultant test statistic as  $D^{(b)}$ .
11:    if  $D^{(b)} > D$  then  $s = s + 1$ 
12:    end for
13:   Output  $s/B$  as an estimated  $p$ -value associated with  $D$  from Step 3.
14: end procedure

```

As indicated in Section 3.1, RoC can be used to test hypotheses about μ , such as testing covariate dependence of it by adopting Algorithm 1 with the restricted MLEs for μ and γ obtained under the current null $H_0^{(\mu)}$. Moreover, because D incorporates information regarding direction comparison between two fitted values of μ besides information relating to concentration comparison that RoC focuses on, one can combine the two test statistics to gain more insight into the underlying data-generating mechanism. If D is significantly larger than RoC when testing covariate dependence of μ , one may interpret it as data evidence for the direction of μ depending on some covariate. Having D close to RoC can imply that the direction of μ may not be dependent on covariates, although its norm may depend on covariates. This exemplifies the versatility and additional insight our proposed test statistics can offer when compared with LR.

4.2 Testing covariates dependence of γ and beyond

Unique to our parameterization of $\text{ESAG}(\mu, \gamma)$, parameters in γ control variation of the distribution in different subspaces on the hypersphere besides (an)isotropy. It is thus of interest to test if such distributional features depend on covariates. For instance, one may consider testing the null $H_0^{(\gamma)} : \mathbf{Y} | \mathbf{X} \sim \text{ESAG}(\mu = \alpha_0 + \mathbf{A}_1 \mathbf{X}, \gamma = \beta_0)$ versus the alternative $H_1 : \mathbf{Y} | \mathbf{X} \sim \text{ESAG}(\mu = \alpha_0 + \mathbf{A}_1 \mathbf{X}, \gamma = \beta_0 + \mathbf{B}_1 \mathbf{X})$. Because γ as a whole relates to (an)isotropy of the distribution, RoC that is initially proposed for testing isotropy has its natural appeal for testing hypotheses about γ . When a violation of $H_0^{(\gamma)}$ adversely affects inferences for μ , the test statistic D designed for testing assumptions on μ also has the potential to detect covariates dependence of γ . With the restricted MLEs $\hat{\mu}_{0i}$ and $\hat{\gamma}_{0i}$ now reflecting $H_0^{(\gamma)}$ used in Algorithm 1 or Algorithm 2, one can carry out the test based on RoC or D to test $H_0^{(\gamma)}$.

Fixing H_1 at the above saturated ESAG model, to test other null hypotheses, say, $\alpha_k = \mathbf{0}$ for a given $k \in \{1, \dots, q\}$, RoC and D can be used with the restricted MLEs in Algorithms 1 and 2 revised accordingly to reflect the specific null hypothesis under consideration. Even if one adopts an angular Gaussian distribution that is not ESAG, as long as the mean vector μ has the same interpretations as that in $\text{ESAG}(\mu, \gamma)$, RoC and D remain meaningful statistics for testing assumptions on μ or other model assumptions that inferences for μ are sensitive to. One simply needs to revise the bootstrap procedures to adapt to the assumed angular Gaussian distribution.

Lastly, RoC and D depend on both the restricted and unrestricted MLEs of model parameters, which in turn add to the computational burden in Algorithms 1 and 2 where these MLEs are obtained based on each bootstrap sample. We thus propose yet another testing strategy that only requires computing the restricted MLEs that is based on a second moment estimation, with the test statistic given by

$$M = \left\| \frac{1}{n} \sum_{i=1}^n \left\{ \mathbf{Y}_i^2 - \widehat{\mathbf{E}}_0(\mathbf{Y}_i^2) \right\} \right\|, \quad (4.2)$$

where \mathbf{Y}_i^2 is the element-wise quantity square of \mathbf{Y}_i , and $\widehat{\mathbf{E}}_0(\mathbf{Y}_i^2)$ is an empirical mean of \mathbf{Y}^2 given $\mathbf{X} = \mathbf{X}_i$ computed using a random sample simulated from an estimated null model $\hat{Q}(\cdot; \hat{\mu}_{0i})$. Unlike RoC and D , the construction of M is

not motivated by (and thus does not target at testing) a particular aspect of the model specification; instead, M can serve as an overall goodness-of-fit test statistic. By construction, in the absence of model misspecification, M is expected to be close to zero, and a larger M serves as data evidence of a poor fit of a null model for the observed data. As an example, Algorithm 3 below gives the algorithm for using M to test the null model that assumes an isotropic ESAG, with an estimated p -value obtained via parametric bootstrap as an output.

Algorithm 3 Hypothesis testing for isotropy based on M defined in (4.2)

```

1: procedure COMPUTE  $M$  BASED ON THE OBSERVED DATA
2:   Input data  $\{(\mathbf{Y}_i, \mathbf{X}_i)\}_{i=1}^n$ , find the restricted MLE  $\hat{\boldsymbol{\mu}}_{0i}$ , for  $i = 1, \dots, n$ .
3:   For  $i = 1, \dots, n$ , generate  $\{\tilde{\mathbf{Y}}_{i,m}\}_{m=1}^{10^4}$  from  $\text{ESAG}(\hat{\boldsymbol{\mu}}_{0i}, \boldsymbol{\gamma}_i = \mathbf{0})$ , compute  $\widehat{\mathbf{E}}_0(\mathbf{Y}_i^2) = 10^{-4} \sum_{m=1}^{10^4} \tilde{\mathbf{Y}}_{i,m}^2$ .
4:   Compute  $M = \|(1/n) \sum_{i=1}^n \{\mathbf{Y}_i^2 - \widehat{\mathbf{E}}_0(\mathbf{Y}_i^2)\}\|$ .
5: end procedure
6: procedure BOOTSTRAP PROCEDURE TO ESTIMATE THE NULL DISTRIBUTION OF  $M$ 
7:   Set  $B =$  number of bootstraps
8:   Initiate  $s = 0$ 
9:   for  $b$  in  $1, \dots, B$  do
10:    Generate the  $b$ -th bootstrap sample  $\{\mathbf{Y}_i^{(b)}\}_{i=1}^n$ , where  $\mathbf{Y}_i^{(b)} | \mathbf{X}_i \sim \text{ESAG}(\boldsymbol{\mu}_i = \hat{\boldsymbol{\mu}}_{0i}, \boldsymbol{\gamma}_i = \mathbf{0})$ , for  $i = 1, \dots, n$ .
11:    Repeat Steps 2–4 using data  $\{(\mathbf{Y}_i^{(b)}, \mathbf{X}_i)\}_{i=1}^n$ . Denote the resultant test statistic as  $M^{(b)}$ .
12:    if  $M^{(b)} > M$  then  $s = s + 1$ 
13:  end for
14:  Output  $s/B$  as an estimated  $p$ -value associated with  $M$  from Step 4.
15: end procedure

```

5 Simulation study

5.1 Design of simulation experiments

We are now in the position to study empirically operating characteristics of the proposed testing procedures for testing $H_0^{(\mathbf{V})}$, $H_0^{(\boldsymbol{\mu})}$, and $H_0^{(\boldsymbol{\gamma})}$ versus the alternative $H_1 : \mathbf{Y} | \mathbf{X} \sim \text{ESAG}(\boldsymbol{\mu} = \boldsymbol{\alpha}_0 + \mathbf{A}_1 \mathbf{X}, \boldsymbol{\gamma} = \boldsymbol{\beta}_0 + \mathbf{B}_1 \mathbf{X})$. To this end, we design several data-generating mechanisms (DGM) for each null hypothesis. A random sample of size $n \in \{200, 400, 800\}$ is generated according to each DGM, based on which the proposed test statistics and their estimated p -values are computed following Algorithms 1–3 with $B = 300$. As a benchmark testing procedure to compare with ours, we also test each null using LR, with the corresponding p -value estimated via parametric bootstrap, as opposed to assuming a χ^2 null distribution for LR as in Paine et al. (2020). This experiment is repeated 200 times at each simulation setting specified by the null hypothesis, DGM, and the level of n . Common in all settings, we consider one covariate, with n realizations $\{X'_i\}_{i=1}^n$ generated from $N(0, 1)$, followed by standardization via $X_i = (X'_i - X'_{(1)}) / (X'_{(n)} - X'_{(1)}) + 1$, for $i = 1, \dots, n$. Given the covariate data $\{X_i\}_{i=1}^n$, response data $\{\mathbf{Y}_i\}_{i=1}^n$ are generated according to a DGM specified in Table 1.

As one can see in Table 1, for each considered null hypothesis, we include a DGM matching the null. This allows for inspecting the size of a test. For each considered null, we also design several DGMs with increasing model complexity compared to the null. The values of some regression coefficients depend on a quantity r that we vary in the simulation to control the severity of model misspecification under a null, with a larger r leading to a more pronounced deviation of the DGM from a null. This allows for monitoring the power of a test as the true model deviates from the null model further.

The metric we record in the simulation study is the relative frequency of a considered test rejecting the current null across 200 Monte Carlo replicates at a pre-specified significance level. In what follows, we present these rejection rates associated with different tests for testing each of the three null hypotheses tabulated in Table 1.

5.2 Simulation results

Figure 2 provides the rejection rates of RoC, D or M , and LR versus the nominal significance level based on data generated from an ESAG regression model consistent with a null hypothesis in Table 1. Focusing on the lower range of the nominal level such as 0.01 and 0.05, we conclude well-controlled sizes of all proposed tests, whereas the size of LRT may be subject to slight inflation, especially when testing covariate dependence of model parameters. This can be where the size of LRT fails to approach the nominal level asymptotically even when its p -value is estimated by the

Table 1: Data-generating mechanisms (DGM) designed for testing each considered null hypothesis regarding ESAG($\boldsymbol{\mu}$, $\boldsymbol{\gamma}$), along with values of model parameters in these DGMs

Null hypothesis	ESAG data-generating mechanism
$H_0^{(\mathbf{V})} : \boldsymbol{\mu} = \boldsymbol{\alpha}_0 + \boldsymbol{\alpha}_1 X, \boldsymbol{\gamma} = \mathbf{0}$	DGM ₀ ^(V) : $\boldsymbol{\mu} = \boldsymbol{\alpha}_0^* + \boldsymbol{\alpha}_1^* X, \boldsymbol{\gamma} = \mathbf{0}$
	DGM ₁ ^(V) : $\boldsymbol{\mu} = \boldsymbol{\alpha}_0^* + \boldsymbol{\alpha}_1^* X, \boldsymbol{\gamma} = \boldsymbol{\beta}_{0r}^*$
	DGM ₂ ^(V) : $\boldsymbol{\mu} = \boldsymbol{\alpha}_0^* + \boldsymbol{\alpha}_1^* X, \boldsymbol{\gamma} = \boldsymbol{\beta}_{0r}^* + \boldsymbol{\beta}_{1r}^* X$
$H_0^{(\boldsymbol{\mu})} : \boldsymbol{\mu} = \boldsymbol{\alpha}_0, \boldsymbol{\gamma} = \boldsymbol{\beta}_0 + \boldsymbol{\beta}_1 X$	DGM ₀ ^(μ) : $\boldsymbol{\mu} = \boldsymbol{\alpha}_0^*, \boldsymbol{\gamma} = \mathbf{0}$
	DGM ₁ ^(μ) : $\boldsymbol{\mu} = \boldsymbol{\alpha}_0^* + \boldsymbol{\alpha}_{1r}^* X, \boldsymbol{\gamma} = \mathbf{0}$
	DGM ₂ ^(μ) : $\boldsymbol{\mu} = \boldsymbol{\alpha}_0^* + \boldsymbol{\alpha}_{1r}^* X, \boldsymbol{\gamma} = \boldsymbol{\beta}_0^*$
	DGM ₃ ^(μ) : $\boldsymbol{\mu} = \boldsymbol{\alpha}_0^* + \boldsymbol{\alpha}_{1r}^* X, \boldsymbol{\gamma} = \boldsymbol{\beta}_0^* + \boldsymbol{\beta}_1^* X$
$H_0^{(\boldsymbol{\gamma})} : \boldsymbol{\mu} = \boldsymbol{\alpha}_0 + \boldsymbol{\alpha}_1 X, \boldsymbol{\gamma} = \boldsymbol{\beta}_0$	DGM ₀ ^(γ) : $\boldsymbol{\mu} = \boldsymbol{\alpha}_0^* + \boldsymbol{\alpha}_1^* X, \boldsymbol{\gamma} = \mathbf{0}$
	DGM ₁ ^(γ) : $\boldsymbol{\mu} = \boldsymbol{\alpha}_0^* + \boldsymbol{\alpha}_1^* X, \boldsymbol{\gamma} = \boldsymbol{\beta}_{1r}^*$
	DGM ₂ ^(γ) : $\boldsymbol{\mu} = \boldsymbol{\alpha}_0^* + \boldsymbol{\alpha}_1^* X, \boldsymbol{\gamma} = \boldsymbol{\beta}_0^* + \boldsymbol{\beta}_{1r}^* X$
Values of model parameters	$\boldsymbol{\alpha}_0^* = (2, -5, 3, 5)^\top,$ $\boldsymbol{\alpha}_1^* = (2, 1, 2, 1)^\top, \boldsymbol{\alpha}_{1r}^* = \frac{r}{2} \mathbf{1}_4,$ $\boldsymbol{\beta}_0^* = (3, 5, -3, -4, 2)^\top, \boldsymbol{\beta}_{0r}^* = \frac{r}{\sqrt{5}} \mathbf{1}_5$ $\boldsymbol{\beta}_1^* = (4, 2, 5, -2, 3)^\top, \boldsymbol{\beta}_{1r}^* = \frac{r}{\sqrt{5}} \mathbf{1}_5$

conventional parametric bootstrap, which is a phenomenon described in [Drton and Williams \(2011\)](#). One shall thus interpret the empirical power of LRT with caution. For this reason, we omit to report the empirical power of LRT for testing covariate dependence.

Table 2 presents the empirical power of various tests for testing each of the three null hypotheses at a significance level of 0.05 based on data from different true ESAG models. When using RoC, M , and LR to test isotropy, the three tests are comparable in their power to detect anisotropy, with the power increasing steadily as n grows bigger or as the true value of $\boldsymbol{\gamma}$ deviates from zero further (by having a larger r). Having a covariate-dependent $\boldsymbol{\gamma}$ in the true regression model also enhances the power of these tests, although M appears to be somewhat less powerful than RoC in this scenario.

According to Table 2, the tests based on RoC and D enjoy higher power to detect covariate dependence of $\boldsymbol{\mu}$ when the true model also has a covariate-dependent $\boldsymbol{\gamma}$ (as in DGM₃^(μ)) than when it has an intercept-only model for $\boldsymbol{\gamma}$ (as in DGM₂^(μ)). Noting that obtaining the unrestricted MLE for $\boldsymbol{\gamma}$ using data from DGM₂^(μ) creates an irregular maximum likelihood estimation, but the same estimation using data from DGM₃^(μ) is a regular case, we believe that having irregular MLEs for model parameters can compromise the power of RoC and D . When testing $H_0^{(\boldsymbol{\gamma})}$, the power of the proposed tests does not increase as quickly as when testing $H_0^{(\boldsymbol{\mu})}$ when n increases or when the covariate dependence becomes stronger. We conjecture that, once we allow $\boldsymbol{\mu}$ to depend on covariates, inferences for the concentration are less sensitive to the assumption of covariate-independent for $\boldsymbol{\gamma}$, and thus RoC and D may lack high power to detect the dependence of $\boldsymbol{\gamma}$ on covariates unless when the dependence is very strong.

The moment-based test using M is much less powerful than the RoC test and the test based on D for testing covariate dependence of model parameters. By solely focusing on the fit for the mean of \mathbf{Y}^2 , the power M to detect model misspecification heavily hinges on the impact of the misspecification on second-moment estimation. The observed phenomenon suggests some level of robustness of the second-moment estimation to covariate dependence of ESAG model parameters. In additional simulation study not reported here where we generate covariate data from different distributions, we observe that likelihood-based estimation of $E(\mathbf{Y}^2)$ is more sensitive to violation of $H_0^{(\boldsymbol{\mu})}$ or $H_0^{(\boldsymbol{\gamma})}$ when the covariate distribution is skewed, and, consequently, M becomes more powerful in detecting covariate dependence of $\boldsymbol{\mu}$ or $\boldsymbol{\gamma}$.

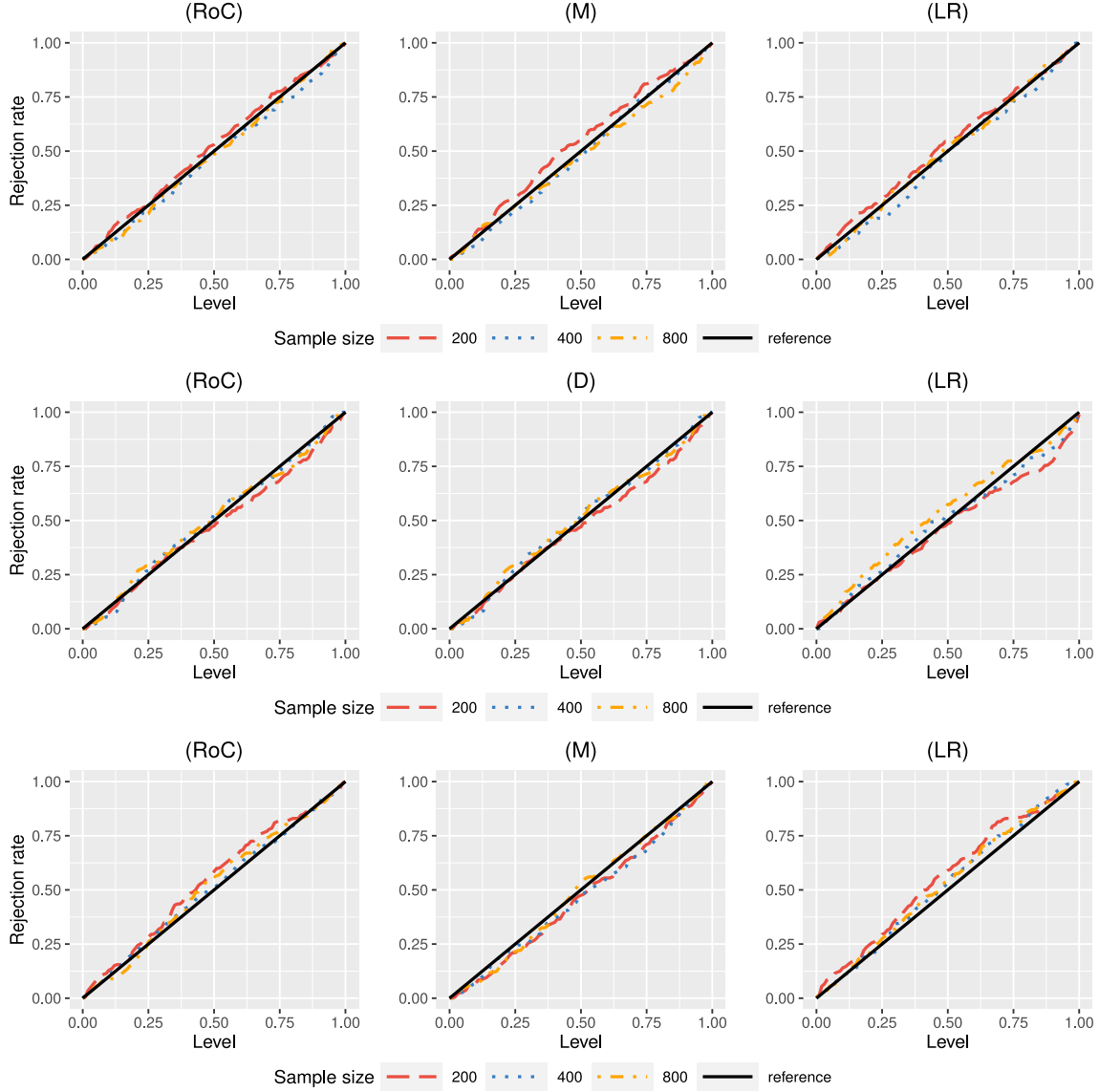


Figure 2: Rejection rates of tests for testing isotropy, $H_0^{(\mathbf{V})}$ (top row), covariate dependence of $\boldsymbol{\mu}$, $H_0^{(\boldsymbol{\mu})}$ (middle row), and covariate dependence of $\boldsymbol{\gamma}$, $H_0^{(\boldsymbol{\gamma})}$ (bottom row) when $n = 200$ (red dashed lines), 400 (blue dotted lines), and 800 (orange dash-dotted lines). The black solid lines are the 45° reference line.

6 Prediction Regions

Following the estimation of all model parameters in an ESAG regression model, one can predict the outcome of the directional response \mathbf{Y} . If all model parameters are known, similar to the prediction region for a multivariate Gaussian distribution (Chew, 1966), a sensible $100(1 - a)\%$ prediction region that reflects the elliptical symmetry of $\text{ESAG}(\boldsymbol{\mu}, \boldsymbol{\gamma})$ is an ellipsoidal ball given by

$$\text{PR}_a = \{ \mathbf{y} \in \mathbb{S}^{d-1} : (\mathbf{y} - \boldsymbol{\mu} / \|\boldsymbol{\mu}\|)^{\top} \mathbf{V}^{-1} (\mathbf{y} - \boldsymbol{\mu} / \|\boldsymbol{\mu}\|) \leq q_a \}, \quad (6.1)$$

where q_a is chosen such that $\text{P}(\mathbf{Y} \in \text{PR}_a) = 1 - a$. We show in Appendix A of the Supplementary Material that PR_a defined in (6.1) has the smallest volume in a class of ellipsoidal prediction regions centering around $\boldsymbol{\mu} / \|\boldsymbol{\mu}\|$ with the nominal coverage probability of $1 - a$.

When the model parameters are unknown, we evaluate $\boldsymbol{\mu}$ and \mathbf{V} at their MLEs, $\hat{\boldsymbol{\mu}}$ and $\hat{\mathbf{V}}$, in (6.1), and estimate q_a by \hat{q}_a that is obtained using bootstrap samples from the estimated ESAG distribution. This leads to a $100(1 - a)\%$

Table 2: Rejection rates associated with different tests for testing $H_0^{(V)}$, $H_0^{(\mu)}$, and $H_0^{(\gamma)}$ at nominal level 0.05

$\{n\}$	200	400	800	200	400	800	200	400	800
Testing $H_0^{(V)} : \mu = \alpha_0 + \alpha_1 X, \gamma = \mathbf{0}$									
	RoC			M			LR		
r	DGM ₁ ^(V) : $\mu = \alpha_0^* + \alpha_1^* X, \gamma = \beta_{0r}^*$								
0.1	0.075	0.110	0.160	0.095	0.105	0.145	0.070	0.100	0.220
0.2	0.145	0.245	0.515	0.145	0.280	0.435	0.145	0.305	0.615
0.4	0.440	0.870	0.995	0.360	0.745	0.935	0.470	0.900	0.995
r	DGM ₂ ^(V) : $\mu = \alpha_0^* + \alpha_1^* X, \gamma = \beta_{0r}^* + \beta_{1r}^* X$								
0.1	0.210	0.420	0.795	0.190	0.390	0.675	0.215	0.470	0.850
0.2	0.675	0.990	1.000	0.525	0.890	1.000	0.710	1.000	1.000
0.4	1.000	1.000	1.000	0.980	1.000	1.000	1.000	1.000	1.000
Testing $H_0^{(\mu)} : \mu = \alpha_0, \gamma = \beta_0 + \beta_1 X$									
	RoC			D			M		
r	DGM ₁ ^(μ) : $\mu = \alpha_0^* + \alpha_{1r}^* X, \gamma = \mathbf{0}$								
0.5	0.075	0.065	0.085	0.055	0.070	0.080	0.005	0.025	0.005
1	0.200	0.265	0.405	0.195	0.240	0.420	0.005	0.025	0.065
2	0.660	0.800	0.935	0.635	0.815	0.965	0.115	0.160	0.345
r	DGM ₂ ^(μ) : $\mu = \alpha_0^* + \alpha_{1r}^* X, \gamma = \beta_0^*$								
0.5	0.440	0.760	0.970	0.350	0.635	0.935	0.075	0.105	0.060
1	0.935	0.995	1.000	0.930	0.995	1.000	0.205	0.160	0.135
2	1.000	1.000	1.000	0.995	1.000	1.000	0.470	0.525	0.590
r	DGM ₃ ^(μ) : $\mu = \alpha_0^* + \alpha_{1r}^* X, \gamma = \beta_0^* + \beta_{1r}^* X$								
0.5	0.850	0.975	1.000	0.745	0.935	1.000	0.140	0.145	0.260
1	1.000	1.000	1.000	1.000	1.000	1.000	0.215	0.240	0.265
2	1.000	1.000	1.000	1.000	1.000	1.000	0.775	0.880	0.935
Testing $H_0^{(\gamma)} : \mu = \alpha_0 + \alpha_1 X, \gamma = \beta_0$									
	RoC			D			M		
r	DGM ₁ ^(γ) : $\mu = \alpha_0^* + \alpha_1^* X, \gamma = \beta_{1r}^* X$								
0.5	0.120	0.090	0.155	0.125	0.090	0.150	0.045	0.035	0.080
1	0.135	0.130	0.185	0.135	0.125	0.185	0.030	0.070	0.065
2	0.145	0.170	0.305	0.155	0.160	0.305	0.070	0.090	0.050
r	DGM ₂ ^(γ) : $\mu = \alpha_0^* + \alpha_1^* X, \gamma = \beta_0^* + \beta_{1r}^* X$								
0.5	0.045	0.055	0.080	0.050	0.050	0.085	0.070	0.075	0.070
1	0.105	0.095	0.160	0.105	0.090	0.160	0.060	0.055	0.045
2	0.165	0.340	0.620	0.165	0.325	0.605	0.065	0.045	0.045

prediction region defined as

$$\widehat{\text{PR}}_a = \left\{ \mathbf{y} \in \mathbb{S}^{d-1} : (\mathbf{y} - \hat{\boldsymbol{\mu}} / \|\hat{\boldsymbol{\mu}}\|)^{\top} \hat{\mathbf{V}}^{-1} (\mathbf{y} - \hat{\boldsymbol{\mu}} / \|\hat{\boldsymbol{\mu}}\|) \leq \hat{q}_a \right\}. \quad (6.2)$$

Algorithm 4 below provides the detailed computational path leading to $\widehat{\text{PR}}_a$ when $\mathbf{X} = \mathbf{x}_0$. Appendix B of the Supplementary Material presents a simulation study where we follow Algorithm 4 to compute prediction regions of different nominal coverage probabilities based on samples of size $n \in \{200, 400, 800\}$. The simulation results suggest that the empirical coverage probabilities of the resultant prediction regions match closely with the nominal levels.

7 Real-life data applications

We now put into action the regression analysis toolkit on data examples from two real-life applications.

7.1 Hydrochemical data

We analyzed in a recent work (Yu and Huang, 2024) the relative abundance of two major ions, K^+ and Na^+ , and two minor ions, Ca^{2+} and Mg^{2+} , in water samples collected from two sets of locations between the summer of 1997 and

Algorithm 4 Compute the prediction region in (6.2)

-
- 1: **procedure** PARAMETRIC BOOTSTRAP ACCOUNTING FOR VARIATION OF ESAG
 - 2: Given the observed data $\{(\mathbf{Y}_i, \mathbf{X}_i)\}_{i=1}^n$, compute the MLEs for regression coefficients, $\hat{\alpha}_0$, $\hat{\mathbf{A}}_1$, $\hat{\beta}_0$, and $\hat{\mathbf{B}}_1$, assuming an ESAG model for \mathbf{Y}_i conditioning on \mathbf{X}_i .
 - 3: Compute $\hat{\boldsymbol{\mu}} = \hat{\alpha}_0 + \hat{\mathbf{A}}_1 \mathbf{x}_0$ and $\hat{\boldsymbol{\gamma}} = \hat{\beta}_0 + \hat{\mathbf{B}}_1 \mathbf{x}_0$, obtain the corresponding $\hat{\mathbf{V}}$.
 - 4: Set m = the number of bootstrap samples. Generate a random sample, $\{\mathbf{Y}'_j\}_{j=1}^m$, from ESAG($\hat{\boldsymbol{\mu}}, \hat{\boldsymbol{\gamma}}$).
 - 5: Compute $q_j = (\mathbf{Y}'_j - \hat{\boldsymbol{\mu}}/\|\hat{\boldsymbol{\mu}}\|)^T \hat{\mathbf{V}}^{-1} (\mathbf{Y}'_j - \hat{\boldsymbol{\mu}}/\|\hat{\boldsymbol{\mu}}\|)$, for $j = 1, \dots, m$.
 - 6: **end procedure**
 - 7: **procedure** NONPARAMETRIC BOOTSTRAP ACCOUNTING FOR VARIATION OF MLES
 - 8: Set B = the number of bootstrap samples.
 - 9: **for** b in $1, \dots, B$ **do**
 - 10: Generate the b -th bootstrap sample $\{\mathbf{Y}_i^{(b)}, \mathbf{X}_i^{(b)}\}_{i=1}^n$ via sampling with replacement from the raw data.
 - 11: Repeat Steps 2–5 using data $\{(\mathbf{Y}_i^{(b)}, \mathbf{X}_i^{(b)})\}_{i=1}^n$. Denote the bootstrap version of q_j as $q_j^{(b)}$.
 - 12: **end for**
 - 13: Viewing $\{q_j, q_j^{(1)}, \dots, q_j^{(B)}\}_{j=1}^m$ as a sample of size $m \times (B + 1)$, find the $(1 - a)$ -quantile of this sample. Denote this sample quantile as \hat{q}_a .
 - 14: Output a $100(1 - a)\%$ prediction region when $\mathbf{X} = \mathbf{x}_0$ given by $\{\mathbf{y} \in \mathbb{S}^{d-1} : (\mathbf{y} - \hat{\boldsymbol{\mu}}/\|\hat{\boldsymbol{\mu}}\|)^T \hat{\mathbf{V}}^{-1} (\mathbf{y} - \hat{\boldsymbol{\mu}}/\|\hat{\boldsymbol{\mu}}\|) \leq \hat{q}_a\}$.
 - 15: **end procedure**
-

the spring of 1999: 67 samples from tributaries of Anioia and 43 samples from tributaries of the lower Llobregat course in Spain (Otero et al., 2005). The complete data are available in the R package, *compositions* (Van den Boogaart and Tolosana-Delgado, 2008). The relative abundance of $(\text{K}^+, \text{Na}^+, \text{Ca}^{2+}, \text{Mg}^{2+})$ is an example of compositional data in a 4-dimensional simplex, $\mathbb{C}^{4-1} = \{\mathbf{y}^* \in \mathbb{R}^4 : \mathbf{1}_4^\top \mathbf{y}^* = 1 \text{ and } \mathbf{e}_j^\top \mathbf{y}^* \geq 0, \text{ for } j = 1, \dots, 4\}$, where $\mathbf{1}_4$ is the 4×1 vector of ones, and \mathbf{e}_j is the unit vector with the j -th entry being 1. We transformed the compositional data by taking the square-root of $\mathbf{y}^* \in \mathbb{C}^{4-1}$ element-wise to directional data in \mathbb{S}^{4-1} . Previous analyses of the directional data from each set of locations suggested an adequate fit of an intercept-only ESAG model, but a poor fit for the combined data of size $n = 110$ from two sets of locations.

These earlier findings motivate a location-dependent ESAG model for all data from these locations, where we incorporate a covariate X indicating locations, with $X = 0$ corresponding to tributaries of Anioia (At), and $X = 1$ representing tributaries of lower Llobregat course (LLt). Fitting the regression model, $Y_i | X_i \sim \text{ESAG}(\boldsymbol{\mu}_i = \boldsymbol{\alpha}_0 + \boldsymbol{\alpha}_1 X_i, \boldsymbol{\gamma}_i = \boldsymbol{\beta}_0 + \boldsymbol{\beta}_1 X_i)$, to the data, we arrive at the following estimates for the ESAG model parameters,

$$\hat{\boldsymbol{\mu}}_i = \begin{bmatrix} 1.99 \\ 5.74 \\ 7.95 \\ 4.59 \end{bmatrix} + \begin{bmatrix} 1.28 \\ 2.83 \\ 1.06 \\ 1.20 \end{bmatrix} X_i, \quad \hat{\boldsymbol{\gamma}}_i = \begin{bmatrix} -0.67 \\ 0.15 \\ -0.82 \\ 6.12 \\ 0.64 \end{bmatrix} + \begin{bmatrix} 2.43 \\ -0.22 \\ 10.17 \\ -20.19 \\ 0.47 \end{bmatrix} X_i.$$

Hence, for the directional response associated with tributaries of Anioia, the mean direction is estimated to be $\hat{\boldsymbol{\mu}}_{\text{At}} = (1.99, 5.74, 7.95, 4.59)^\top$, and, for the directional response coming from tributaries of lower Llobregat course, the estimated mean direction is $\hat{\boldsymbol{\mu}}_{\text{LLt}} = (3.27, 8.57, 9.01, 5.79)^\top$. These estimates lead to the estimated concentration at each set of locations, which suggests that the latter set of locations exhibits a higher concentration than the former. These are coherent with results in our previous analysis when we analyzed data from one set of locations at a time. Estimates for $\boldsymbol{\gamma}_i$ when $X_i = 0$ and 1 are also aligned with our earlier analyses (and are omitted here), based on which estimates of \mathbf{V} for two sets of locations, $\hat{\mathbf{V}}_{\text{At}}$ and $\hat{\mathbf{V}}_{\text{LLt}}$, can be obtained.

For model diagnosis, we carry out tests for isotropy and covariate dependence of $\boldsymbol{\mu}$ and $\boldsymbol{\gamma}$ based on the three proposed test statistics. All tests suggest statistically significant evidence of location-dependent model parameters in the ESAG distribution that is anisotropic for the (transformed) compositions of $(\text{K}^+, \text{Na}^+, \text{Ca}^{2+}, \text{Mg}^{2+})$, with all estimated p -values less than 10^{-3} except for that associated with M when testing covariate dependence of $\boldsymbol{\gamma}$, which returns an estimated p -value less than 0.01 (although larger than 10^{-3}). This is consistent with findings in existing literature reporting that the hydrochemical profile of Anioia and that of the Llobregat lower course are substantially different because the two sets of tributaries pass through zones that are differently populated with vastly different distributions of agricultural and industrial areas (González et al., 2012). Looking more closely at the test statistics when testing covariate dependence of $\boldsymbol{\mu}$, i.e., testing the null $H_0^{(\boldsymbol{\mu})}$, we have $D = 1.062$ that is somewhat higher than $\text{RoC} = 1.059$. This can be data evidence indicating that not only the norm of the mean direction depends on X , that is, the concentration varies across locations, but also the orientation of the mean direction differs between locations. When testing covariate dependence of $\boldsymbol{\gamma}$, i.e., testing $H_0^{(\boldsymbol{\gamma})}$ versus the full model, the two statistics are nearly equal (at around

1.090). This suggests that, once we acknowledge a location-dependent $\boldsymbol{\mu}$ in the null model, allowing $\boldsymbol{\gamma}$ to depend on X in the alternative model mostly helps to distinguish the variability of data across different locations but it may not contribute to capturing the discrepancy in the orientation of $\boldsymbol{\mu}$ in different locations.

Lastly, applying Algorithm 4 for $x_0 = 0$ and 1, we obtain the prediction regions for the two sets of locations given by

$$\begin{aligned}\widehat{\text{PR}}_a^{(\text{At})} &= \{\mathbf{y} \in \mathbb{S}^3 : (\mathbf{y} - \hat{\boldsymbol{\mu}}_{\text{At}} / \|\hat{\boldsymbol{\mu}}_{\text{At}}\|)^{\top} \hat{\mathbf{V}}_{\text{At}}^{-1} (\mathbf{y} - \hat{\boldsymbol{\mu}}_{\text{At}} / \|\hat{\boldsymbol{\mu}}_{\text{At}}\|) \leq \hat{q}_a^{(\text{At})}\}, \\ \widehat{\text{PR}}_a^{(\text{LLt})} &= \{\mathbf{y} \in \mathbb{S}^3 : (\mathbf{y} - \hat{\boldsymbol{\mu}}_{\text{LLt}} / \|\hat{\boldsymbol{\mu}}_{\text{LLt}}\|)^{\top} \hat{\mathbf{V}}_{\text{LLt}}^{-1} (\mathbf{y} - \hat{\boldsymbol{\mu}}_{\text{LLt}} / \|\hat{\boldsymbol{\mu}}_{\text{LLt}}\|) \leq \hat{q}_a^{(\text{LLt})}\},\end{aligned}$$

with the estimated $(1 - a)$ -quantiles given by $\hat{q}_a^{(\text{At})} = 0.029, 0.036, 0.050$ and $\hat{q}_a^{(\text{LLt})} = 0.018, 0.023, 0.031$, for $a = 0.7, 0.8, 0.9$, respectively. At each considered nominal level, having $\hat{q}_a^{(\text{LLt})} < \hat{q}_a^{(\text{At})}$ is in line with the finding that the distribution of directional data from the lower Llobregat course exhibits a higher concentration (i.e., lower variability) than that for Anoià.

7.2 Microbiome data

We now turn to a dataset regarding the gut microbiota of elderly adults. Besides gut microbiome compositions of 160 elderly adults, also recorded in this data include the residence types, age, body mass index (BMI), diet, and gender. A similar dataset has been analyzed by [Claesson et al. \(2012\)](#), where the authors carried out a principal component analysis to study correlations of the relative abundance of various microorganisms in the gut. [Shen et al. \(2022\)](#) used the Gaussian chain graph model for the data to infer the effects of one's diet and residence type on gut microbiome composition. For illustration purposes, we study the potential association between two covariates, one's age and BMI, and the directional response on \mathbb{S}^3 defined as the square root of the relative abundance of four genera of bacteria found in the gut: Blautia, Caloramator, Clostridium, and Faecalibacterium.

We first fit the directional response data to the ESAG regression model, for $i = 1, \dots, 160$,

$$\mathbf{Y}_i | (\text{Age}_i, \text{BMI}_i) \sim \text{ESAG}(\boldsymbol{\mu}_i = \boldsymbol{\alpha}_0 + \boldsymbol{\alpha}_1 \text{Age}_i + \boldsymbol{\alpha}_2 \text{BMI}_i, \boldsymbol{\gamma}_i = \boldsymbol{\beta}_0 + \boldsymbol{\beta}_1 \text{Age}_i + \boldsymbol{\beta}_2 \text{BMI}_i), \quad (7.1)$$

where $\mathbf{Y}_i = (Y_{i,1}, Y_{i,2}, Y_{i,3}, Y_{i,4})^{\top}$, with $Y_{i,j}$ equal to the squared root of the relative abundance of Blautia, Caloramator, Clostridium, and Faecalibacterium, for $j = 1, 2, 3, 4$, respectively, for subject i , $\text{Age}_i = (\text{subject } i\text{'s age} - \text{the youngest subject's age}) / (\text{age range}) + 1$, and BMI_i is similarly computed by standardizing the BMI data. Maximum likelihood estimation yields

$$\begin{aligned}\hat{\boldsymbol{\mu}}_i &= \begin{bmatrix} 1.76 \\ 0.62 \\ 5.27 \\ 3.23 \end{bmatrix} + \begin{bmatrix} -1.46 \\ 0.59 \\ -2.70 \\ -2.93 \end{bmatrix} \text{Age}_i + \begin{bmatrix} 1.11 \\ -0.63 \\ 1.63 \\ 2.39 \end{bmatrix} \text{BMI}_i, \\ \hat{\boldsymbol{\gamma}}_i &= \begin{bmatrix} -6.39 \\ 0.31 \\ 3.12 \\ 0.63 \\ 0.69 \end{bmatrix} + \begin{bmatrix} 24.08 \\ 2.54 \\ -4.29 \\ -3.31 \\ 0.61 \end{bmatrix} \text{Age}_i + \begin{bmatrix} -21.15 \\ -2.35 \\ 3.07 \\ 3.20 \\ -0.79 \end{bmatrix} \text{BMI}_i.\end{aligned} \quad (7.2)$$

We first carry out the residual-based goodness-of-fit test proposed in an earlier work ([Yu and Huang, 2024](#)). We showed there that, if $\mathbf{Y} \sim \text{ESAG}(\boldsymbol{\mu}, \boldsymbol{\gamma})$, then $T = (\|\boldsymbol{\mu}\|^2 + \sum_{j=1}^d \lambda_j) \mathbf{r} \mathbf{V}^{-1} \mathbf{r}$ follows χ_{d-1}^2 approximately, where $\lambda_1 \leq \lambda_2 \leq \dots \leq \lambda_{d-1}$ and $\lambda_d = 1$ are the eigenvalues of \mathbf{V} , and $\mathbf{r} = (\mathbf{I}_d - \hat{\mathbf{Y}} \hat{\mathbf{Y}}^{\top}) \mathbf{Y}$ is the directional residual ([Jupp, 1988](#)) associated with the prediction $\hat{\mathbf{Y}} = \hat{\boldsymbol{\mu}} / \|\hat{\boldsymbol{\mu}}\|$. Figure 3 shows the residual-based quantities T evaluated at the MLEs of unknown parameters, $\{\hat{T}_i\}_{i=1}^{160}$, where $\hat{T}_i = (\|\hat{\boldsymbol{\mu}}_i\|^2 + \sum_{j=1}^3 \hat{\lambda}_{i,j} + 1) \mathbf{r}_i \hat{\mathbf{V}}_i^{-1} \mathbf{r}_i$. In particular, the empirical distribution of T depicted by the histogram of $\{\hat{T}_i\}_{i=1}^{160}$ appears to resemble χ_3^2 , even though the scatter plots of $\{\hat{T}_i\}_{i=1}^{160}$ versus the covariates values seem to suggest several outliers in the sample. To estimate the null distribution of T without approximating its distribution by χ_{d-1}^2 , the authors also developed a bootstrap-based test for assessing the adequacy of an ESAG model. This test applied to the current dataset yields an estimated p -value of 0.58, suggesting insufficient evidence for the lack of fit of the current model. In addition, the tests for isotropy based on RoC and M , and the tests for covariates dependence of ESAG model parameters based on RoC and D all produce estimated p -values less than 0.01. We thus conclude significant covariates effects on the ESAG model parameters and recommend against opting for a regression model more parsimonious than (7.1).

To further elucidate the effects of age and BMI on ESAG model features, we present in Figure 4 estimates of the concentration and three eigenvalues of \mathbf{V} , $(\lambda_1, \lambda_2, \lambda_3)$, versus BMI when one is 70, 80, and 90 years of age. As age

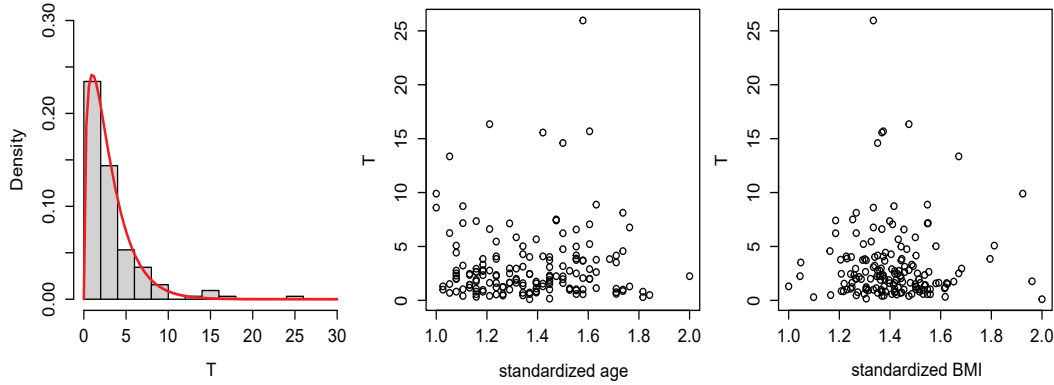


Figure 3: The histogram of $\{\hat{T}_i\}_{i=1}^{160}$ with the density of χ_3^2 superimposed (in the left panel), the scatter plot of $\{(\text{Age}_i, \hat{T}_i)\}_{i=1}^{160}$ (in the middle panel), and the scatter plot of $\{(\text{BMI}_i, \hat{T}_i)\}_{i=1}^{160}$ (in the right panel) based on microbiome data modeled by (7.1).

increases, we observe in Figure 4 a decrease in the estimate of $\|\mu\|$, corresponding to an increase in the estimated overall variation of \mathbf{Y} . The finding of highly variable directional distribution can imply highly variable in the composition of the gut microbiota among the elderly, which is a finding reported in existing literature but has been mostly stated in comparison with younger (than 65) healthy adults that are found to have a more stable composition of intestinal microorganisms (Claesson et al., 2012). Our results here can be evidence for that, even among the elderly, the trend of higher variability in microbiome composition as one ages persists. In addition, a higher BMI also leads to a more variable distribution. Examining the estimated eigenvalues of \mathbf{V} , one can see two change points in BMI: one at BMI of nearly 25 for an 80-year-old and the other at BMI of around 35 for a 90-year-old. The first change point separates healthy weight (BMI $\in (18.5, 24.9)$) and overweight (BMI $\in (25.0, 29.9)$); the second change point belongs to the obese range (<https://www.cdc.gov/healthyweight/assessing>). Because $\lambda_1 = \lambda_2 = \lambda_3 = 1 (= \lambda_4)$ implies $\mathbf{V} = \mathbf{I}_4$, the proximity of the three considered eigenvalues to 1 implies isotropy of the directional distribution and also relates to the correlations between the four genera of bacteria. The aforementioned change points are where the estimates for these eigenvalues are closest to 1, and thus the distribution of \mathbf{Y} tends to be more isotropic when $\mathbf{X} = (\text{Age} = 80, \text{BMI} \approx 25)$ and $(\text{Age} = 90, \text{BMI} \approx 35)$. This can also imply a reduction in the correlation between the relative abundance of the four considered genera of bacteria at these change points.

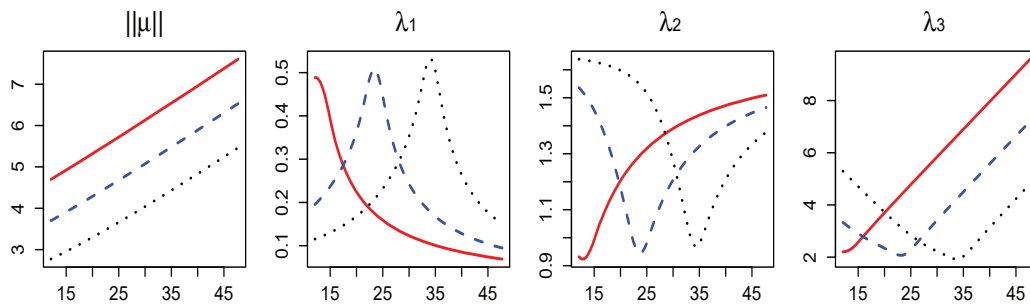


Figure 4: Estimates of $\|\mu\|$, λ_1 , λ_2 , and λ_3 versus BMI when one is 70 (red solid lines), 80 (blue dashed lines), and 90 (black dotted lines) years of age.

8 Discussion

We develop in this study a complete package of regression analysis for directional response built upon the ESAG distribution family indexed by constraint-free parameters. We consider a full range of statistical inference problems,

including parameter estimation, testing hypotheses on model features, and prediction. The uncertainty of parameter estimation can be assessed via bootstrap. Parametric bootstrap is also heavily involved in all proposed inference procedures, which is straightforward to implement owing to the formulation and parametrization of ESAG that allow for easy data generation from an ESAG distribution. Computer programs for implementing all proposed methods are available at https://github.com/Zehaoyu217/ESAG/blob/main/ESAG_Project2.R. We also demonstrate the use of this package for analyzing two datasets from different fields of applications.

The number of parameters in an ESAG regression model can be large in an application since the dimensionality of the parameter space grows quadratically in the dimension of \mathbf{Y} , d , and linearly in the number of covariates, q . For example, in microbiome analysis, d is the dimension of the compositional response, which typically is much larger than four, and one may wish to consider many covariates relating to the host's physiological characteristics. We have started developing penalized likelihood-based methods to deal with high-dimensional directional data. Besides this ongoing follow-up research, another interesting topic is compositional data analysis that the two case studies in Section 7 relate to. The idea of relating compositional data on a simplex to directional data on a hypersphere has been explored (Scealy and Welsh, 2011, 2017; Li et al., 2023) but with many open questions yet to be addressed. In this particular context, more components may have zero or nearly zero relative abundance as d increases, which is a data pattern ESAG and most existing named directional distributions tend to fit poorly. Interpretations and implications of model parameters of a directional distribution that are practically meaningful for the corresponding compositional data also demand further systematic investigation.

References

- Banerjee, A., Dhillon, I. S., Ghosh, J., Sra, S., and Ridgeway, G. (2005). Clustering on the unit hypersphere using von Mises-Fisher distributions. *Journal of Machine Learning Research*, 6(9).
- Chernoff, H. (1954). On the distribution of the likelihood ratio. *The Annals of Mathematical Statistics*, 25(3):573–578.
- Chew, V. (1966). Confidence, prediction, and tolerance regions for the multivariate normal distribution. *Journal of the American Statistical Association*, 61(315):605–617.
- Claesson, M. J., Jeffery, I. B., Conde, S., Power, S. E., O’connor, E. M., Cusack, S., Harris, H., Coakley, M., Lakshminarayanan, B., O’sullivan, O., et al. (2012). Gut microbiota composition correlates with diet and health in the elderly. *Nature*, 488(7410):178–184.
- Drton, M. (2009). Likelihood ratio tests and singularities. *The Annals of Statistics*, 37(2):979–1012.
- Drton, M. and Williams, B. (2011). Quantifying the failure of bootstrap likelihood ratio tests. *Biometrika*, 98(4):919–934.
- Ennajari, H., Bouguila, N., and Bentahar, J. (2021). Combining knowledge graph and word embeddings for spherical topic modeling. *IEEE Transactions on Neural Networks and Learning Systems*, 34(7):3609–3623.
- González, S., López-Roldán, R., and Cortina, J.-L. (2012). Presence and biological effects of emerging contaminants in Llobregat River basin: a review. *Environmental Pollution*, 161:83–92.
- Johnson, R. A. and Wehrly, T. E. (1978). Some angular-linear distributions and related regression models. *Journal of the American Statistical Association*, 73(363):602–606.
- Jupp, P. (1988). Residuals for directional data. *Journal of Applied Statistics*, 15(2):137–147.
- Li, B., Yoon, C., and Ahn, J. (2023). Reproducing kernels and new approaches in compositional data analysis. *Journal of Machine Learning Research*, 24(327):1–34.
- Lund, U. (1999). Least circular distance regression for directional data. *Journal of Applied Statistics*, 26(6):723–733.
- Mitchell, J. D., Allman, E. S., and Rhodes, J. A. (2019). Hypothesis testing near singularities and boundaries. *Electronic journal of statistics*, 13(1):2150.
- Otero, N., Tolosana-Delgado, R., Soler, A., Pawlowsky-Glahn, V., and Canals, A. (2005). Relative vs. absolute statistical analysis of compositions: a comparative study of surface waters of a Mediterranean river. *Water research*, 39(7):1404–1414.
- Paine, P. J., Preston, S., Tsagris, M., and Wood, A. T. (2020). Spherical regression models with general covariates and anisotropic errors. *Statistics and Computing*, 30(1):153–165.
- Paine, P. J., Preston, S. P., Tsagris, M., and Wood, A. T. (2018). An elliptically symmetric angular Gaussian distribution. *Statistics and Computing*, 28(3):689–697.
- Presnell, B., Morrison, S. P., and Littell, R. C. (1998). Projected multivariate linear models for directional data. *Journal of the American Statistical Association*, 93(443):1068–1077.
- Ryali, S., Chen, T., Supekar, K., and Menon, V. (2013). A parcellation scheme based on von mises-fisher distributions and markov random fields for segmenting brain regions using resting-state fmri. *Neuroimage*, 65:83–96.
- Scealy, J. and Welsh, A. (2011). Regression for compositional data by using distributions defined on the hypersphere. *Journal of the Royal Statistical Society: Series B (Statistical Methodology)*, 73(3):351–375.
- Scealy, J. and Welsh, A. (2017). A directional mixed effects model for compositional expenditure data. *Journal of the American Statistical Association*, 112(517):24–36.
- Scealy, J. and Wood, A. T. (2019). Scaled von Mises–Fisher distributions and regression models for paleomagnetic directional data. *Journal of the American Statistical Association*.
- Shen, Y., Solís-Lemus, C., and Deshpande, S. K. (2022). Sparse Gaussian chain graphs with the spike-and-slab LASSO: Algorithms and asymptotics. *arXiv preprint arXiv:2207.07020*.
- Van den Boogaart, K. G. and Tolosana-Delgado, R. (2008). “compositions”: a unified R package to analyze compositional data. *Computers & Geosciences*, 34(4):320–338.
- Wang, F. and Gelfand, A. E. (2013). Directional data analysis under the general projected normal distribution. *Statistical Methodology*, 10(1):113–127.
- White, H. (1982). Maximum likelihood estimation of misspecified models. *Econometrica*, 50(1):1–25.
- Yu, Z. and Huang, X. (2024). A new parameterization for elliptically symmetric angular gaussian distributions of arbitrary dimension. *Electronic Journal of Statistics*, 18(1):301–334.

Web Appendix A: Prediction regions of the smallest volume

Suppose $\mathbf{Y} \sim \text{ESAG}(\boldsymbol{\mu}_0, \gamma_0)$ resulting from normalizing $\mathbf{W} \sim \mathcal{N}_d(\boldsymbol{\mu}_0, \mathbf{V}_0)$. Define a class of $100(1 - a)\%$ prediction regions $\{\text{PR}_a(\mathbf{V}) : \mathbf{V}$ is a $d \times d$ positive definite matrix satisfying $\mathbf{V}\boldsymbol{\mu}_0 = \boldsymbol{\mu}_0$ and $\det(\mathbf{V}) = 1\}$, where

$$\text{PR}_a(\mathbf{V}) = \{\mathbf{y} \in \mathbb{S}^{d-1} : (\mathbf{y} - \boldsymbol{\mu}_0/\|\boldsymbol{\mu}_0\|)^\top \mathbf{V}^{-1}(\mathbf{y} - \boldsymbol{\mu}_0/\|\boldsymbol{\mu}_0\|) \leq q_a\}, \quad (\text{A.1})$$

with q_a chosen such that $P(\mathbf{Y} \in \text{PR}_a(\mathbf{V})) = 1 - a$. In what follows, we show that $\text{PR}_a(\mathbf{V}_0)$ has the smallest volume in this class.

Because

$$\begin{aligned} & (\mathbf{Y} - \boldsymbol{\mu}_0/\|\boldsymbol{\mu}_0\|)^\top \mathbf{V}^{-1}(\mathbf{Y} - \boldsymbol{\mu}_0/\|\boldsymbol{\mu}_0\|) \\ &= \mathbf{Y}^\top \mathbf{V}^{-1} \mathbf{Y} - 2 \frac{\boldsymbol{\mu}_0^\top}{\|\boldsymbol{\mu}_0\|} \mathbf{V}^{-1} \mathbf{Y} + \frac{\boldsymbol{\mu}_0^\top}{\|\boldsymbol{\mu}_0\|} \mathbf{V}^{-1} \frac{\boldsymbol{\mu}_0}{\|\boldsymbol{\mu}_0\|} \\ &= \mathbf{Y}^\top \mathbf{V}^{-1} \mathbf{Y} - 2 \frac{\boldsymbol{\mu}_0^\top}{\|\boldsymbol{\mu}_0\|} \mathbf{Y} + 1, \text{ since } \boldsymbol{\mu}_0^\top \mathbf{V}^{-1} = \boldsymbol{\mu}_0^\top, \end{aligned}$$

which depends on \mathbf{V} only via $\mathbf{Y}^\top \mathbf{V}^{-1} \mathbf{Y}$. We further elaborate on this term next. With $\mathbf{Y} = \mathbf{W}/\|\mathbf{W}\|$, we re-express \mathbf{Y} as $(\mathbf{V}_0^{1/2} \mathbf{Z} + \boldsymbol{\mu}_0)/\|\mathbf{W}\|$, where $\mathbf{Z} \sim \mathcal{N}_d(\mathbf{0}, \mathbf{I}_d)$. It follows that

$$\begin{aligned} & \mathbf{Y}^\top \mathbf{V}^{-1} \mathbf{Y} \\ &= \frac{\mathbf{Z}^\top \mathbf{V}_0^{1/2} \mathbf{V}^{-1} \mathbf{V}_0^{1/2} \mathbf{Z} + 2 \boldsymbol{\mu}_0^\top \mathbf{V}^{-1} \mathbf{V}_0^{1/2} \mathbf{Z} + \boldsymbol{\mu}_0^\top \mathbf{V}^{-1} \boldsymbol{\mu}_0}{\|\mathbf{W}\|^2} \\ &= \frac{\mathbf{Z}^\top \mathbf{V}_0^{1/2} \mathbf{V}^{-1} \mathbf{V}_0^{1/2} \mathbf{Z} + 2 \boldsymbol{\mu}_0^\top \mathbf{V}_0^{1/2} \mathbf{Z} + \|\boldsymbol{\mu}_0\|^2}{\|\mathbf{W}\|^2}, \end{aligned}$$

which depends on \mathbf{V} only via $\mathbf{Z}^\top \mathbf{V}_0^{1/2} \mathbf{V}^{-1} \mathbf{V}_0^{1/2} \mathbf{Z} = \mathbf{Z}^\top \mathbf{G} \mathbf{Z}$, where $\mathbf{G} = \mathbf{V}_0^{1/2} \mathbf{V}^{-1} \mathbf{V}_0^{1/2}$. Because $\det(\mathbf{V}_0) = \det(\mathbf{V}) = 1$, \mathbf{G} is a symmetric positive definite matrix with a determinant equal to one.

Note that q_a is affected by \mathbf{V} via the variation of $\mathbf{Z}^\top \mathbf{G} \mathbf{Z}$. To show that $\text{PR}_a(\mathbf{V}_0)$ has the smallest volume in the class of prediction regions defined above, it suffices to show that $\text{Var}(\mathbf{Z}^\top \mathbf{Z}) \leq \text{Var}(\mathbf{Z}^\top \mathbf{G} \mathbf{Z})$. Because $\mathbf{Z}^\top \mathbf{Z} \sim \chi_d^2$, $\text{Var}(\mathbf{Z}^\top \mathbf{Z}) = 2d$. Using the eigendecomposition of \mathbf{G} given by \mathbf{PDP}^\top , we have

$$\begin{aligned} \text{Var}(\mathbf{Z}^\top \mathbf{G} \mathbf{Z}) &= \text{Var}(\mathbf{Z}^\top \mathbf{PDP}^\top \mathbf{Z}) \\ &= \text{Var}(\mathbf{U}^\top \mathbf{D} \mathbf{U}), \text{ where } \mathbf{U} = (U_1, \dots, U_d)^\top = \mathbf{P} \mathbf{Z} \sim \mathcal{N}_d(\mathbf{0}, \mathbf{I}_d), \\ &= \sum_{j=1}^d D_j^2 \text{Var}(U_j^2), \text{ where } D_j \text{ is the } j\text{-th diagonal entry of } \mathbf{D}, \\ &= 2 \sum_{j=1}^d D_j^2, \text{ since } U_j^2 \sim \chi_1^2, \text{ for } j = 1, \dots, d, \end{aligned}$$

where $D_j > 0$, for $j = 1, \dots, d$, and $\prod_{j=1}^d D_j = \det(\mathbf{G}) = 1$. By the arithmetic–geometric mean inequality,

$$\frac{1}{d} \sum_{j=1}^d D_j^2 \geq \left(\prod_{j=1}^d D_j^2 \right)^{1/d},$$

with the right-hand side equal to one since $\prod_{j=1}^d D_j^2 = \prod_{j=1}^d D_j = 1$. Hence, $\sum_{j=1}^d D_j^2 \geq d$, and thus $\text{Var}(\mathbf{Z}^\top \mathbf{G} \mathbf{Z}) \geq \text{Var}(\mathbf{Z}^\top \mathbf{Z})$.

In conclusion, setting $\mathbf{V} = \mathbf{V}_0$ so that $\mathbf{G} = \mathbf{I}_d$ results in the lowest variation in $(\mathbf{Y} - \boldsymbol{\mu}_0/\|\boldsymbol{\mu}_0\|)^\top \mathbf{V}^{-1}(\mathbf{Y} - \boldsymbol{\mu}_0/\|\boldsymbol{\mu}_0\|)$, which leads to the smallest value of q_a , and further leads to the smallest volume for the prediction region.

Web Appendix B: Simulation study on prediction regions

For illustration purposes, we carry out a simulation study where we implement Algorithm 4 to construct prediction regions based on random samples of size $n \in \{200, 400, 800\}$ from an ESAG model with intercept-only models for

both μ and γ , with $\mu = (2, -5, 3, 5)^\top$ and $\gamma = (3, 5, -3, 4, 2)^\top$. Following constructing a prediction region based on a random sample, we compute the proportion of the sample falling in this region, viewed as an empirical coverage probability of the prediction region.

Table 3 provides Monte Carlo averages of the empirical coverage probabilities across 2000 Monte Carlo replicates at each simulation setting specified by the level of n . These summary statistics suggest satisfactory performance of the proposed prediction region in that they achieve the desired coverage probabilities even when the sample size is moderate.

Table 3: Monte Carlo averages of empirical coverage probabilities associated with prediction regions at three nominal levels $1 - \alpha$. Numbers in parentheses are Monte Carlo standard errors of corresponding averages.

$1 - \alpha$	$n = 200$	$n = 400$	$n = 800$
0.90	0.895 (0.0174)	0.897 (0.0121)	0.898 (0.0089)
0.95	0.947 (0.0111)	0.948 (0.0080)	0.949 (0.0058)
0.99	0.989 (0.0350)	0.989 (0.0026)	0.990 (0.0019)